Engineering Structures 166 (2018) 376–386

Contents lists available at ScienceDirect

Engineering Structures

journal homepage: www.elsevier.com/locate/engstruct

Computational assessment of the seismic behavior of steel stairs

X. Wang*, T.C. Hutchinson

Dept. of Structural Engineering, Univ. of California, San Diego, La Jolla, CA 92093-0085, United States

ARTICLE INFO

Keywords:
Finite element analysis
Nonstructural components and systems
Seismic behavior
Seismic analysis
Steel stairs

ABSTRACT

Stairs are an essential nonstructural system within buildings, providing egress to occupants as well as much needed access for emergency responders following an extreme event, such as an earthquake. Unfortunately, past earthquakes continue to reveal that these displacement-sensitive systems are highly vulnerable to damage and collapse. In this paper, high fidelity finite element models are developed and exercised in an effort to advance understanding of the seismic behavior of steel stairs under pseudo-static displacement loading indicative of earthquake-induced building movements. The proposed modeling approach is first validated through comparison with a set of experimental data and subsequently extended into a parametric study to broaden the range of stair configurations and details. In particular, the effect of story height, connection and landing details, and geometry on the behavior of the system is studied. Parametric analysis results indicate that the static force and displacement response of the stairs are sensitive to these key design parameters. Importantly, stair-to-buidling connections are subjected to large stress and strain demands under lateral displacement loading, as such their capability to maintain connectivity during an earthquake is crucial for robust seismic performance and hence continued functionality of the stair as a system.

1. Introduction

Stairs are a primary means of egress in buildings. They must remain operable following a strong-intensity earthquake and any ensuing post-earthquake events to support occupant evacuation and emergency response [1,2]. Stairs typically span from floor to floor in a building and therefore are subject to multiple-support dynamic excitations induced by the building during an earthquake. However, their structural response is complex due to the variability in spatial geometry, material, and construction details. Stiff and heavy stairs may even detrimentally interact with the supporting structure and thus modify the seismic response of the supporting structure [3]. Although stairs within a building virtually perform as structural systems from the design perspective, they are often considered within the category of nonstructural components in practice. The seismic design strength of a stair system may be readily estimated using code provisions [4], however their seismic performance is more significantly dictated by the differential displacements induced by their multiple attachment points to the building. Detailing stair systems with sufficient deformability to accommodate the expected floor-to-floor seismic drifts, however, remains a challenge due to limited knowledge regarding their structural behavior under lateral loading. This is further complicated by their complex geometries and variations of specific connection details in practice. As a result, stair systems continued to suffer severe damage and even collapsed in past earthquakes (e.g., [5–8]). Indeed, earthquake-induced damage to stairs continues to cause disruption of building functionality, delayed rescue operations, and even life safety hazards.

Experimental investigations of the seismic behavior of stair systems have occurred only in a few recent efforts. These studies include pseudo-static component tests of full-height reinforced concrete straight-run stairs [9] and full-scale prefabricated steel stairs in a scissors configuration [10]. In addition, a recent shake table test program investigates the system-level seismic behavior of a prefabricated stair system installed within a full-scale building [11,12]. These studies have advanced the state of understanding regarding the seismic behavior of stair systems. Research of this kind, however, is limited in occurrence due to its tremendous cost. To complement these experimental efforts, computational studies are important as they offer a cost-effective alternative to expand experimental findings. Recent computational studies have incorporated stair systems into numerical modeling of the seismic response of buildings in an effort to understand the effect of the stair system on the building response (e.g., [13,14]). It is noted, however, that the capability of the models to capture the seismic response of stairs in a system-level numerical simulation, in particular when the stairs are subjected to significant inelastic deformation during high-intensity earthquake excitations, has not been extensively investigated. Moreover, any effort to conduct numerical simulations requires validation against experiments, however the previous paucity in such data

* Corresponding author.
E-mail addresses: xiw002@ucsd.edu (X. Wang), tara@ucsd.edu (T.C. Hutchinson).

https://doi.org/10.1016/j.engstruct.2018.03.074
Received 26 September 2017; Received in revised form 8 February 2018; Accepted 26 March 2018

has precluded an expanse in numerical simulations as well.

To this end, this paper presents a comprehensive computational study to investigate the seismic behavior of prefabricated steel stairs using detailed three-dimensional finite element models. The models are implemented using the general-purpose finite element software *LS-DYNA* [15,16]. It is noted that a rather rigorous three-dimensional finite element modeling strategy is adopted in an effort to comprehensively capture subtle behavioral aspects of the stair as a system, when key design parameters are varied. The objectives of this study are: (1) to develop finite element models of prefabricated steel stairs that are capable of capturing their global response and local behavior as well as validate the effectiveness of the modeling strategies via comparisons with prior experimental studies [10], and (2) to conduct a parametric assessment of the seismic behavior of prefabricated steel stairs considering a broad range of design parameters commonly found in practice.

The present study focuses on the seismic behavior of the stairs under uniaxial pseudo-static displacement loading. It is assumed that the effect of dynamic loading does not substantially impact the stair response during an earthquake, and as such equivalent static cyclic displacement loading may be applied, due to the following two considerations: (1) the fundamental frequencies of these steel stairs are likely much higher than those of multi-story buildings, thus avoiding excessive acceleration amplification of the stairs [11], and (2) the dynamic inertial forces of these light-weight stairs is small compared with the pseudo-static forces induced by differential displacements. As such, the implications of heavier stairs or stairs with natural frequencies more closely tuned with that of its supporting building are outside of the scope of the present paper. In addition, it is noted that although the stairs are subjected to bi-directional (or tri-directional) floor-to-floor differential displacements during real earthquakes, the scope of the present study is focused on understanding their critical response characteristics under uniaxial displacement loading applied in the horizontal directions. The effects of multi-directional earthquake loading may be the subjects of future studies.

2. Model description

Although stairs vary in aspects such as geometric configuration and construction material, prefabricated steel stairs in a scissors configuration are considered as the prototype stairs in this study. This type of stair system is commonly used in practice and characterized by complex structural behavior, in particular torsional response. Moreover, the prefabricated scissors-type steel stairs were investigated in two recent experimental studies [10,11]. These experiments offer a baseline configuration and other aspects of the prototype stairs considered in the present numerical study. As shown in Fig. 1, the prototype stair consists of a mid-level landing and two parallel flights running in opposite directions from the landing to the upper and lower floors. These components are convenient as they can be assembled in-situ using bolted or welded connections at the floor and landing locations. In addition, the presence of handrails on the stair is optional pending the position of the stair relative to other architectural features. The finite element models of the stairs are implemented in *LS-DYNA* as a detailed three-dimensional representation, which explicitly incorporate all the stair components and connections. As summarized in Table 1, different components or connections fabricated using steel with distinct sectional or material properties (e.g., thickness, steel designation) are considered as different parts in the model. Interested readers are referred to [10] for additional details regarding the prototype stair specimen.

Due to the paucity in material test data, these numerical simulations employ the expected (most probable) steel strengths, which are estimated by scaling the corresponding nominal (specified minimum) steel strengths. The scale factors, referred to as expected yield stress ratio R_y or tensile strength ratio R_t in current design provisions [17], are determined based on statistical survey of a large set of material properties [18]. The reported nominal strengths of steel used in the prototype stair model and the corresponding scale factors are summarized in Table 2.

In the proposed model, material nonlinearity is considered assuming elasto-plastic behavior of the steel materials, whereas geometric nonlinearities are accounted for through small-strain large-displacement element formulations. To prevent unrealistic nodal and element penetrations, contact interfaces are implemented wherever potential contact between adjacent components may occur (e.g., surface-to-surface contact for connection plates bearing against the boundary or the other plate). The static coefficient of friction between steel-to-steel contact surfaces is taken as 0.5 in this numerical study. Additional modeling details of individual components (e.g., flights, landing) and connections (e.g., flight-to-landing and flight-to-building connections), the material models, and the boundary conditions are discussed in subsequent sections.

2.1. Stair components

The flight stringers are fabricated using ASTM A36 plate, while the treads and risers are made of ASTM A786 checkered plate (Fig. 2a). All parts of the flights are modeled using four-node fully integrated shell elements (element type 16 in *LS-DYNA*). A refined mesh region with shell element edge lengths ranging from 12.7 mm (0.5 in.) to 25.4 mm (1 in.) is used at both ends of the flight, since large strain and stress gradients are expected in such regions, while the remaining region employs a coarser mesh with a typical element edge length of approximately 50.8 mm (2 in.) to reduce the computational costs. Cyclic plasticity material models (material type 125 in *LS-DYNA*) are used to model the inelastic stress-strain response of steel in the refined-mesh regions (two ends of the flight), while elastic materials are used in the coarse-mesh regions (mid-span). Simulation results (not shown herein for brevity) confirm that the stress level at the flight mid-span regions attains only about 30% of the yield strength at the ultimate loading state (2.5% interstory drift), therefore justifying the use of elastic materials in these regions.

The landing posts and joists are all constructed using ASTM A36 steel (Fig. 2b). Similar to the flight treads and risers, the landing deck is made of ASTM A786 checkered plate. The landing posts are each connected to a joist using two 16 mm diameter ASTM A307 hex head bolts at the top and bolted to steel members at the bottom. The entire landing is modeled using four-node fully integrated shell elements and cyclic plasticity material models. Comparable to those of the flight refined mesh regions, the edge lengths of the landing shell elements range from 12.7 mm (0.5 in.) to 25.4 mm (1 in.).

2.2. Connections

The flights are attached to the building floors at one end and the landing joist at the other end using ASTM A36 plates or angles. It is noted that connection details differ significantly depending on their location on the stair and the boundary details of the supporting structure. For example, Fig. 3a and b present the flight-to-steel member connections of the prototype stair, in which the connection plate and the angle are both bolted to the steel boundary members using two ASTM A325 tension control bolts per connection. As such, surface-to-surface contact is associated with elements on the contact interface to account for the bearing effect of the boundary. All connection plates or angles are shop-welded to the flight stringers using vertical fillet welds at the two ends of the plate or angle.

These connections are modeled using four-node fully integrated shell elements and cyclic plasticity material models. Since large inelastic deformations with complex stress-strain behavior are expected to concentrate at the connections during the lateral loading, the connections are modeled using a refined mesh with a typical shell element edge length of 12.7 mm (0.5 in.). The welds are represented using penalty-based tie contact that rigidly constrains all translational and

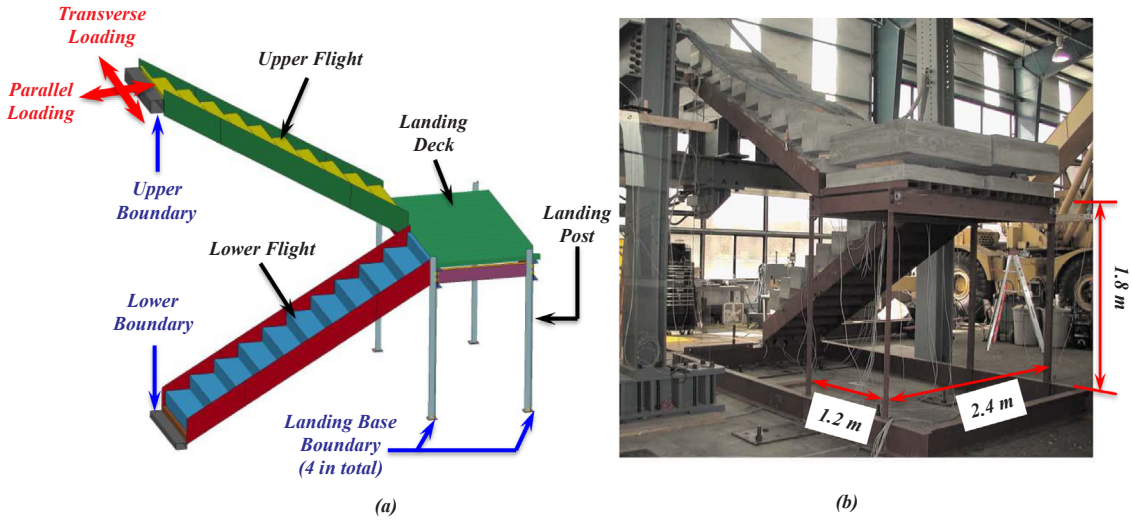

Fig. 1. Prototype prefabricated steel stair (modeled after tests in [10]): (a) three-dimensional finite element model, and (b) test specimen and setup.

Table 1
Stair components and the associated element formulations.

Components and parts		Product description	Element type
Flight	Stringer	A36 plate	Fully integrated shell element[a]
	Tread and riser	A786 checkered plate	
Landing	Post	A36 angle	
	Joist	A36 channel	
	Deck	A786 checkered plate	
Connection plate		A36 plate	
Connection angle		A36 angle	
Flight-to-landing or flight-to-building connection bolts		A325 tension control bolt	Spot weld beam element[b]
Landing post-to-joist connection bolts		A307 hex head bolt	

[a] Shell element type 16 in *LS-DYNA*.
[b] Beam element type 9 in *LS-DYNA*.

Table 2
Material nominal strengths and the associated scale factors of the steel products.

ASTM designation	A36	A786	A325	A307
f_y (MPa) [scale factor]	250 [1.3]	230 [1.3]	n/a	n/a
f_u (MPa) [scale factor]	400 [1.2]	415 [1.2]	830 [1.1]	415 [1.1]

Notes: pre-tension of A325 and A307 bolts is considered as 70% of their ultimate tensile strengths.

rotational degrees-of-freedom for the nodes along the welding joints. In this regard, the models do not intend to directly capture connection weld fracture and instead use the local stress strain response along the welds to assess the connection performance (see Section 2.5 for further discussions). The connection bolts (Fig. 3a and b) are modeled using beam elements with the spot-weld material model (material type 100 in *LS-DYNA*). This material model is capable of applying the initial stress (pre-tension force) to the connection bolt (70% ultimate strength of the bolts). Simulation results indicate that the bolt pre-tension forces fluctuate only slightly (< 10%) during displacement loading, which is corroborated by the experimental observations that the stair connection bolts sustained no apparent damage [10]. In addition, two rigidly constrained node sets are implemented on each end of the bolt, with the node on the bolt defined as the master node and the remaining nodes on the bearing plate as the slave nodes (Fig. 3c). These constrained node sets allow bolt pre-tension to be transferred onto the bearing plates. Surface-to-surface contact is implemented on the bearing plates to model the friction mechanism, which provides resistance to gravity loads of the stair system.

2.3. Material models

For the stair landing and flights modeled using shell elements, a two-surface cyclic plasticity model (material type 125 in *LS-DYNA*) with combined isotropic-kinematic hardening rules [19] is used to capture the material inelasticity. Fig. 4 presents the monotonic and cyclic stress-strain response of ASTM A36 steel (with an expected yield strength f_y of 325 MPa and expected tensile strength f_u of 520 MPa). These results are obtained using a shell element under uniaxial displacement loading. Since material test data for the stair specimens were unavailable in this study, the steel strain corresponding to the ultimate strength is defined as 0.15, according to the test results of similar steel materials reported in the literature (e.g., [20]). It is noted that the cyclic plasticity model provides more reasonable hysteretic behavior compared to the commonly used J2 plasticity model (material type 024 in *LS-DYNA*), since it considers the Bauschinger effect and the stiffness deterioration as a function of plastic strain history. While the two material models provides consistent stress-strain responses under monotonic loading (Fig. 4a), the J2 plasticity model tends to overestimate the material strength and cause sharp transitions under cyclic loading, in particular when the material is subjected to large inelastic cyclic deformation (Fig. 4b).

2.4. Boundary conditions

As shown in Fig. 1, the prototype stair is attached to its supporting structure (test fixture) at multiple locations: (1) the upper flight attached to the upper floor boundary, (2) the lower flight attached to the lower floor boundary, (3) the landing posts attached to the lower floor at their base. To replicate the loading condition in the model, a prescribed displacement history is applied at the upper floor boundary, while the lower floor boundary and the base of the landing posts are fixed. It is also noted that pre-tension on the connection bolts and gravity loads are applied prior to imposition of displacement loading.

2.5. Modeling limitations

Connection weld fracture of steel stairs represents a major damage

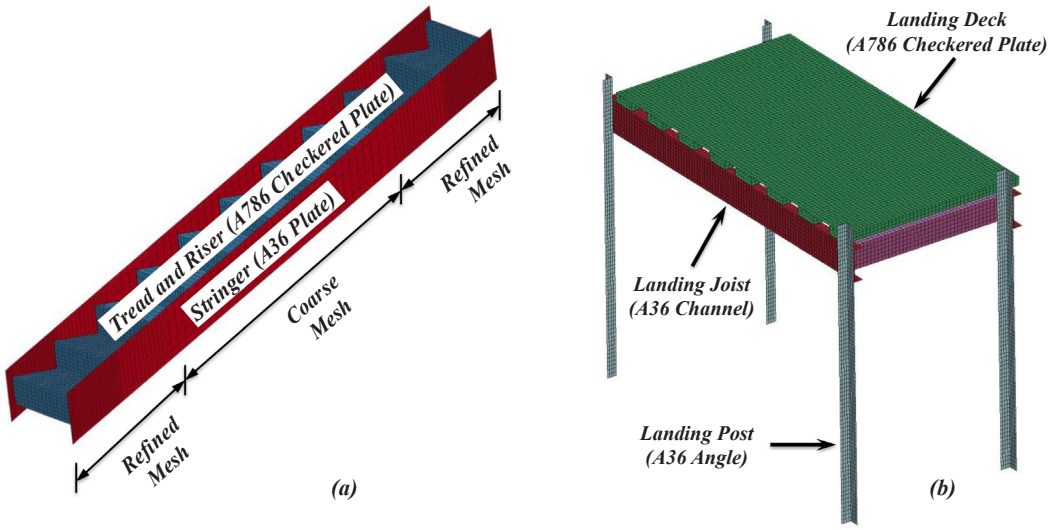

Fig. 2. Stair components: (a) flight, and (b) landing (note that the components are shown separately only for illustrative purposes).

mode and thus largely controls the ultimate deformation capacity of the stairs during intense earthquakes [10,11]. Despite its significance, modeling of weld fracture under large inelastic cyclic loading often relies heavily on well-defined low-cycle fatigue rules and material properties of the welds and base metal (e.g., [21,22]). Absent test data on the specific welded connections, the weld fracture behavior is not explicitly considered in the proposed modeling strategies. Instead, the penalty-based tie contact (rigid type constraint) is employed to constrain the nodes along the welds. Since this modeling strategy implicitly neglects the weld strength deterioration due to load-induced progressive damage (e.g., crack propagation), the simulation results tend to overestimate the lateral force demands of the stair as well as the connection stress and strain responses in the vicinity of the welds. Despite these limitations, the simulated stress and strain responses may remain useful for comparative assessment of the fracture potential for different connection details [23,24]. Mesh sensitivity issues are therefore studied by simulating the stair connection response under uniaxial tension and compression loading. The simulation results, although not presented for brevity, confirm that the global force-displacement and local stress-strain response remain consistent irrespective of the mesh size, thereby justifying the use of stress and strain results for evaluating the connection performance [25].

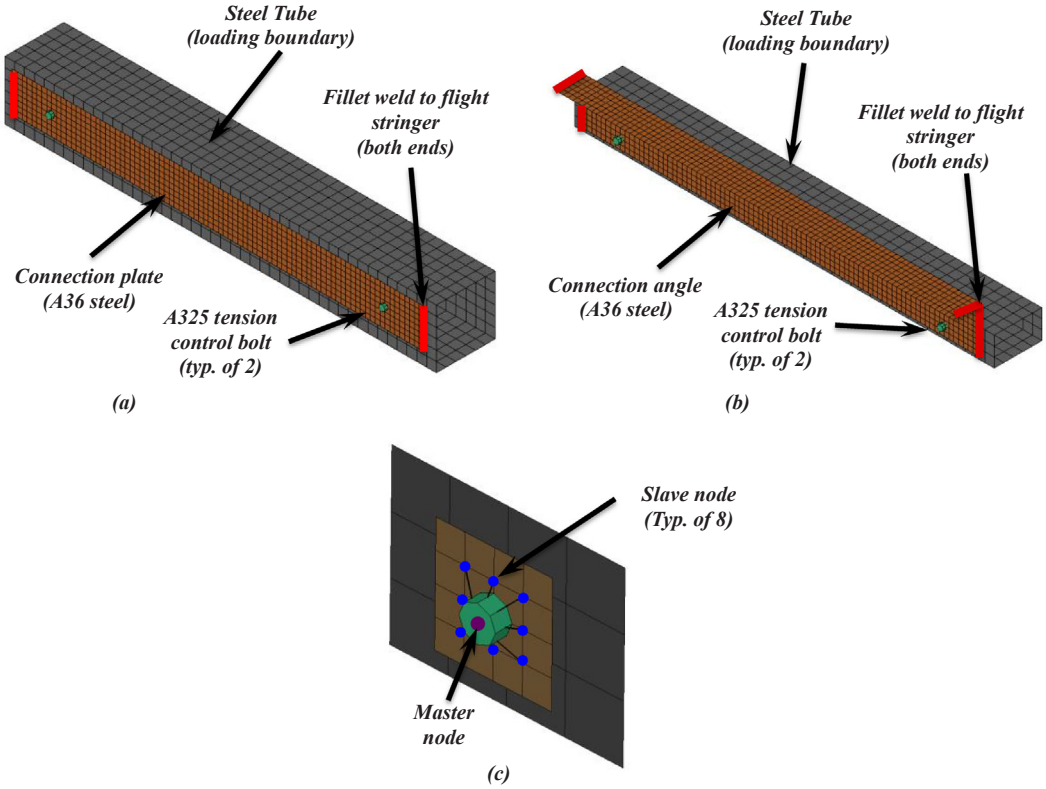

Fig. 3. Stair connections: (a) upper connection, (b) lower connection, and (c) connection bolt.

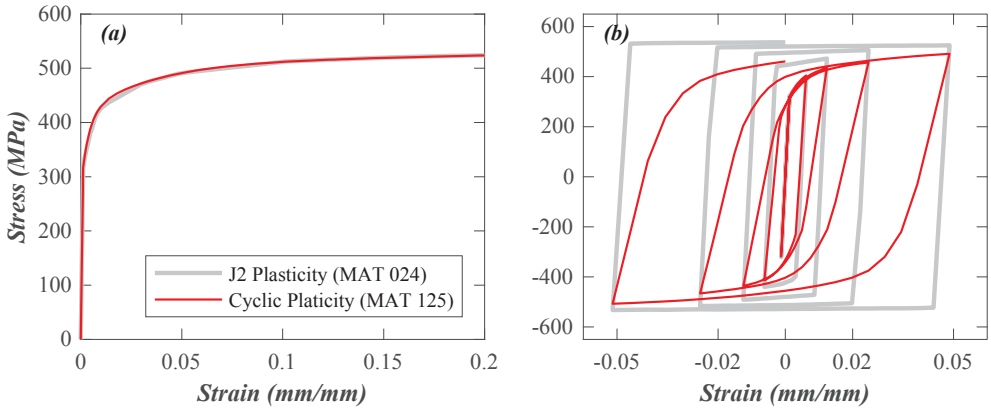

Fig. 4. Uniaxial stress-strain curves of A36 steel: (a) monotonic loading, and (b) cyclic loading.

3. Model validation

The efficacy of the proposed modeling approach is evaluated through comparisons with a prior experimental study on two full-size prefabricated steel stair assemblies using cyclic pseudo-static displacement loading protocol [10]. Since the two specimens demonstrated similar behavior during the tests, the present numerical validation study focuses only on the checkered plate test specimen. This specimen had a height of 3.6 m (assumed story height) and a self weight of 6.5 kN. In addition, a total weight of 25.4 kN (concrete blocks as shown in Fig. 1b) was evenly distributed on the stair treads and landing deck to simulate live loads with a load combination factor of 1.0 (i.e., 100% live load). It is noted that this factor is larger than the code-prescribed factor (0.5 for live loads in seismic load combinations). The pseudo-static cyclic displacements were sequentially applied on the upper boundary of the specimen in the two horizontal directions, which contained progressively increasing amplitudes up to the target displacement in each direction. Compatible with code-prescribed seismic drift demands for multi-story moment frame buildings, the target displacement was defined as an interstory drift ratio (IDR) of 2.5% [4]. Following the completion of the primary loading tests, the specimen was also subjected to additional displacement loading cycles with reduced amplitudes (half of the ultimate displacement) to evaluate the stair behavior in the event of earthquake aftershocks. Additional information regarding the test program and results are available in [10].

To replicate the experimental protocol, displacements in the two loading directions are applied sequentially to account for the impact of damage accumulated at the completion of the first loading direction (transverse to stair run) on the stair response during the subsequent loading direction (in parallel with stair run). As demonstrated in Fig. 5, the simulated hysteretic force-displacement behavior correlates well with the test results in both loading directions, while the force differences are only about 10% even under large displacement range (IDR > 1%). Importantly, the model is capable of capturing the larger lateral force demands when the stair is loaded in the parallel direction. In addition, the salient hysteretic characteristics such as stiffness degradation and pinching are also well captured, although the simulation results slightly overestimate the energy dissipation as evident by larger hysteresis loops in the case of parallel loading (Fig. 5b). The predicted hysteretic energy dissipation under the 2.5% IDR (largest) displacement cycles is about 20% larger than that measured experimentally. This might partially be attributed to the inability of the model to consider progressive weld strength deterioration or bolt loosening under large displacement cycles.

Fig. 6 illustrates the numerically predicted deformed shapes of the stair assembly at the ultimate target displacement (91 mm or an IDR of 2.5%) in the two horizontal loading directions. When the imposed displacement in the parallel direction (pushing the upper flight) achieves the ultimate target, the predicted landing displacement is 109 mm in the parallel direction and 81 mm in the transverse direction (Fig. 6a). In contrast, transverse loading imposes a landing displacement of 30 mm or less in both the longitudinal and transverse directions (Fig. 6b). Therefore, the model effectively represents the prominent characteristics of the stair displacement patterns as observed in the experiments, namely, larger displacement demands in the case of parallel loading and comparable amplitude of landing displacements in the two horizontal directions. The predicted peak landing displacement of 109 mm under parallel loading (about 1.2 time the ultimate drift demand) agrees well with the recommended gap size as found in the experimental study [10].

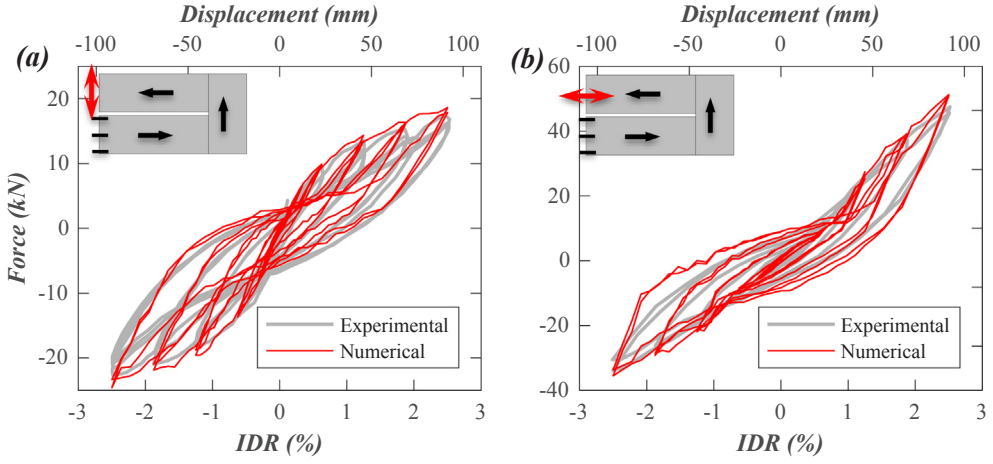

Fig. 5. Force-displacement response of the component-level cyclic loading tests [9]: (a) transverse loading (initial loading direction), and (b) parallel loading (subsequent loading direction) (double-headed red arrow on the upper left schematic indicates the direction of loading; whereas the single-headed black arrows indicate the slope upwards direction). (For interpretation of the references to color in this figure legend, the reader is referred to the web version of this article.)

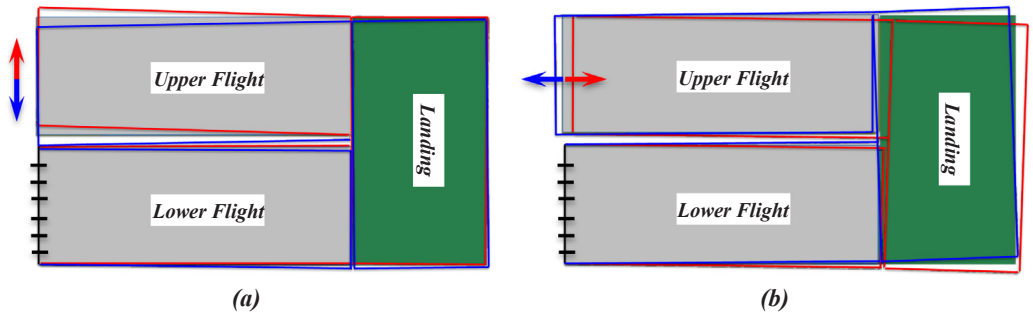

Fig. 6. Deformed shapes of the stair assembly at the ultimate displacement (2.5% IDR) loading as predicted using the model: (a) transverse (initial loading) direction, and (b) parallel (subsequent loading) direction (arrow denotes loading direction).

Table 3
Test matrix of the prefabricated steel stair models in the parametric studies (primary variables compared with the *Baseline Model* are highlighted in **bold font**).

Case[a]	Story height (m)	Landing post	Connection details[b]	Stair configuration
Case 1 (BL)	**3.6**	**L2.5 × 2.5 × 1/4 (bolted)**	**Type-I**	**Scissor**
Case 2 (C2)	**4.2**	L2.5 × 2.5 × 1/4 (bolted)	Type-I	Scissor
Case 3 (C3)	**4.8**	L2.5 × 2.5 × 1/4 (bolted)	Type-I	Scissor
Case 4 (C4)	3.6	**L2.5 × 2.5 × 1/4 (welded)**	Type-I	Scissor
Case 5 (C5)	3.6	**HSS3 × 3 × 1/4 (welded)**	Type-I	Scissor
Case 6 (C6)	3.6	L2.5 × 2.5 × 1/4 (bolted)	**Type-II**	Scissor
Case 7 (C7)	3.6	L2.5 × 2.5 × 1/4 (bolted)	**Type-III**	Scissor
Case 8 (C8)	3.6	L2.5 × 2.5 × 1/4 (bolted)	Type-I	**Straight**

[a] Case 1 represents *Baseline Model*.
[b] See Fig. 3 for Type-I connection details and Fig. 7 for Type-II and Type-III connection details (all flight-to-landing connections are identical).

4. Parametric studies

Using the validated modeling approach, a parametric investigation is conducted to assess the seismic behavior of prefabricated steel stairs with a wider range of design variables commonly found in practice. As described in Table 3, the parametric study includes a total of eight stair models, namely, a *Baseline Model* (Case 1) that resembles the component-level test specimen [10] and seven design variant models that are derived from the *Baseline Model* by modifying one of the four sets of design variables: story height (Cases 2 and 3), landing post (Cases 4 and 5), connection details (Cases 6 and 7), and geometric stair run configuration (Case 8). Regarding the connection details, the *Baseline Model* (Case 1) is identified as that most representative of a condition where the stair is attached to steel members (Fig. 3), while model Case 6 reflects typical concrete floor connections that are stitch welded to boundary embeds (Fig. 7a and c). These two sets of connection details both incorporate a yielding mechanism on the upper connections to accommodate the expected seismic interstory drift demands. In contrast, model Case 7 is intended to represent an extreme condition whereby rigid connections are adopted at both the lower and upper floors, differing substantially from model Case 6 most notably due to the absence of reduced areas within the upper connection angle (Fig. 7b). In addition, the lower connections of the stairs all employ rigid connections with limited deformability (Fig. 7c). Finally, one stair in straight-run configuration (Case 8) is incorporated in the parametric study to evaluate its contrast in response compared with the scissors assemblies. It is noted that the mid-height landing width of the straight-run stair is half that of the scissors stairs.

In the present parametric study, nonlinear static analyses are conducted to obtain the force-displacement behavior of the stairs under monotonic uniaxial displacement loading. The lateral displacement is imposed at the upper floor boundary until the stair attains an IDR of 2.5% (conforming to ASCE-7 code provisions [4]), while the lower floor boundary and the base of the landing posts are all fixed. Consistent with the experimental study [10], 100% live loads are applied to the stairs to represent the above-design level gravity loads. Although not shown for brevity, simulation results indicate that the stair force displacement response and the local connection behavior do not appear sensitive to the variation of live load amplitudes (within the range of 0%–100% live loads) in the case of static displacement loading. However, further experimental studies are recommended to validate this computational finding and moreover assess this impact under simulated earthquake loading.

4.1. Baseline model

Performance parameters for characterizing the stair force-displacement behavior under monotonic static displacement loading are illustrated in Fig. 8a. The yield state is determined as the initial yielding of the critical stair connections (e.g., upper flight-to-floor connections) when the von-Mises stress exceeds the yield stress (Fig. 8b). The stair stiffness K_e is then defined as the secant stiffness when the lateral force attains half the initial yield force. The ultimate state represents the attainment of the peak target displacement corresponding to 2.5% interstory drift (Fig. 8c). The overstrength factor Ω is then defined as the ratio between the ultimate strength F_u and yield strength F_y. It is noted that the ultimate strength F_u indicates the force at the ultimate state as opposed to the peak strength, since the lateral force of the stair increases monotonically without the occurrence of strength deterioration even until the ultimate drift of 2.5% is attained. Other performance parameters include the landing displacements $\Delta_{long}^{landing}$ and $\Delta_{trans}^{landing}$ (relative to lower floor) at the ultimate state (2.5% IDR), since they are critical for determining the gap size in order to avoid undesirable impacts between the stair and the surrounding enclosure.

Fig. 9 presents the lateral force-displacement response of the *Baseline Model* in the two loading directions as well as the landing displacement trajectories. The corresponding performance parameters of the *Baseline Model* are summarized in Table 4. It is noted that the parameters associated with positive loading may differ from those of negative loading (e.g., landing displacement). This is because the non-symmetric geometry of the stairs in a scissors configuration leads to distinct deformation patterns and contact mechanisms between

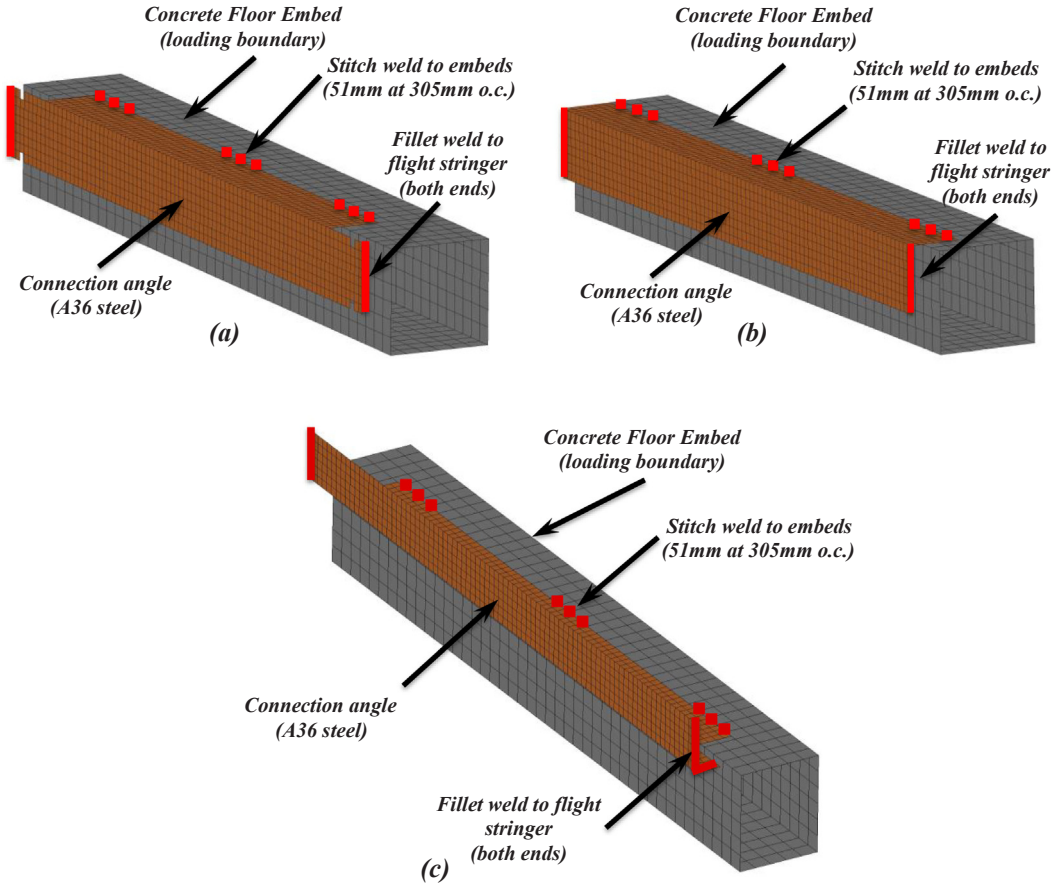

Fig. 7. Stair connections of variant models: (a) upper connection with reduced section at each end of connection angle (Type II), (b) upper connection without reduced section (Type III), and (c) rigid lower connection (Type II and Type III).

separate components. As summarized in the table, the initial stiffness and yield force of the stair for parallel loading appear moderately larger than those for transverse loading. Connection plate initial yielding occurs at an IDR of about 0.3% for parallel loading and 0.4–0.5% for transverse loading, which implies that initial yielding may occur even during a low-amplitude earthquake when the building response remains elastic. At the ultimate state (2.5% IDR), parallel loading imposes apparently larger lateral force and landing displacement demands. As a result, the overstrength factors for parallel loading (about 5) are much larger than those achieved during transverse loading (as much as 3). It is also evident in Fig. 9b that the landing displacement pattern varies significantly for loading in the two directions. Parallel loading imposes considerable torsion on the landing with a diagonal trajectory and comparable displacement components in the two directions, whereas the landing moves primarily in the transverse direction in the case of transverse loading.

To further explore the stair behavior due to the variation in loading directions, the upper floor connection deformations and stringer axial forces of the *Baseline Model* at the ultimate state (2.5% IDR) are compared in Fig. 10. Parallel loading induces elongation at both ends of the

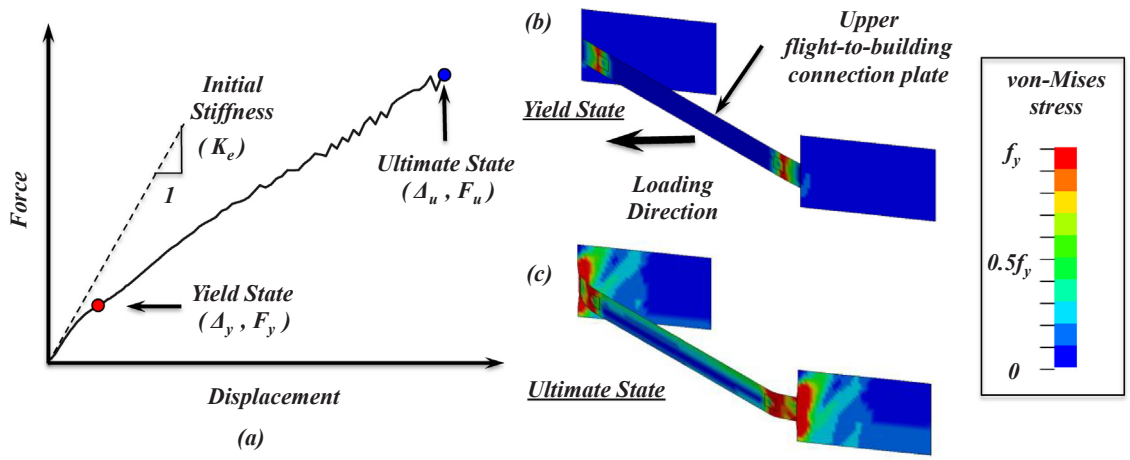

Fig. 8. Illustration of the performance parameters: (a) lateral force-displacement curve (*Baseline Model* under parallel loading), and the von-Mises stress distribution of upper flight-to-building connection under (b) yield state and (c) ultimate state.

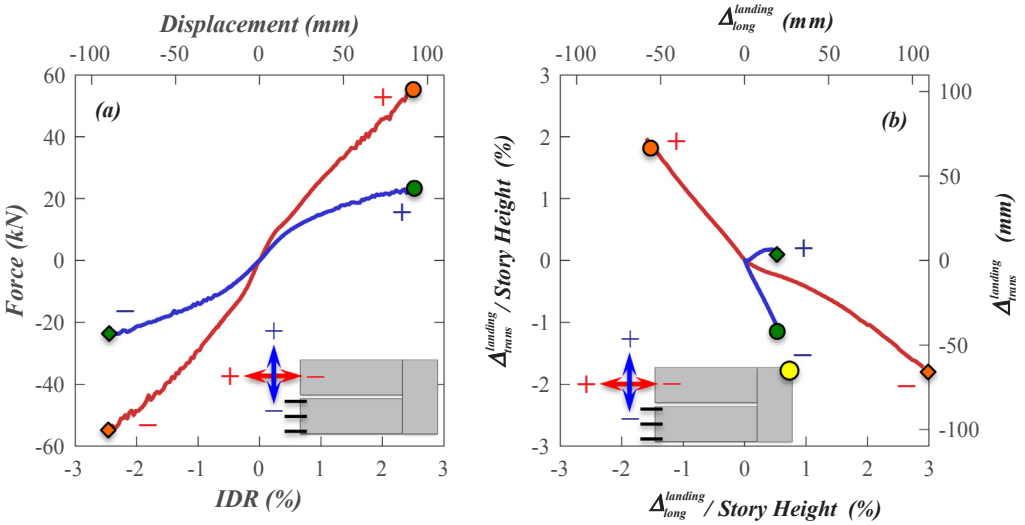

Fig. 9. *Baseline Model* responses under loading in two horizontal directions: (a) lateral force-displacement response, and (b) bi-directional landing corner displacement trajectory (yellow dot indicates the landing corner location). (For interpretation of the references to color in this figure legend, the reader is referred to the web version of this article.)

connection plate with similar amplitude. The average elongation of the connection is about 32 mm at the ultimate state, which account for more than one third of the total story drift (91 mm). In addition, the upper flight resembles an inclined axial member when subject to loading parallel to the run, and the stringers at both sides are subjected to tensile forces of comparable magnitude (Fig. 10a). In the case of transverse loading, however, the connection undergoes deformation in opposite directions at the two ends. While the exterior stringer end elongates by 26 mm at the ultimate state, the interior stringer moves in contact with the loading boundary and is therefore subject to compression (Fig. 10b). Although the prescribed displacement is applied in the transverse direction, the stringer axial forces impose large bending moment and longitudinal force on the loading boundary. The bending moment allows the upper flight to deform as a flexural member, thus effectively enhancing the overall deformability of the stair assembly. In addition, parallel loading induces larger stress and strain demands on the vertical fillet welds at the two ends of the connection plate, with an effective plastic strain of ~0.03 and a principal stress of ~400 MPa.

Although not the primary focus of this study, eigenvalue analyses are conducted to study the vibration characteristics of the *Baseline Model* and their implications in dynamic loading effects. It is noted that the stair mass incorporated into the models excludes those used to represent the live loads, since they are considered as unattached mass. The eigenvalue results indicate that the first two predominant vibration modes correspond to the transverse-to-stair-run vibration at a frequency of 7.7 Hz and the parallel-to-stair-run vibration at a frequency of 19.3 Hz, respectively [25]. The effective modal mass of each mode accounts for more than two thirds of the stair mass in the corresponding direction of vibration. It is noted that the frequency range of these modes is more likely to coincide with the higher mode frequencies as opposed to the fundamental frequency of a typical multi-story building. Consequently, it is reasonable to assume that the dynamic loading effect would not substantially impact the seismic response of these light-weight stairs.

4.2. Force-displacement response

Fig. 11 presents the performance parameters of the seven design variant stair models (see Table 3) normalized by that of the *Baseline Model*. The results are categorized into the four sets of design variables and the two loading directions. As shown in Fig. 11a and b, the story height has the most significant effect on the transverse landing displacements, since the increased landing post height reduces the lateral stiffness of the landing as well as the entire stair assembly. In the case of transverse loading, the increase of story height significantly reduces the initial stiffness and yield force. This is due to the fact that the stair response under parallel loading is strongly dependent on the connection behavior, while its response under the transverse loading is predominately affected by the flexural deformation of the upper flight. As indicated by Fig. 11c and d, while the use of stiffer landing posts (hollow structural sections in Case 5) slightly increases the stiffness and lateral force, it effectively reduces the landing displacements in both horizontal directions. Fig. 11e and f demonstrate that the performance parameters appear much more sensitive to the variations of connection details compared to the former two design variables (e.g., story height and landing post configuration). The initial stiffness, yield force, and landing displacements range as low as half those of the *Baseline Model* for the model with deformable upper connection (Case 6) and twice as high for the one with rigid upper connection (Case 7). The straight-run stair (Case 8) observes smaller stiffness and larger yield displacement demands under transverse loading, since its deformation mechanism differs fundamentally from that of the *Baseline Model* (Fig. 11g and h). It is also important to note that, when the straight-run stair is subjected to compression in the case of parallel loading, the flights perform as inclined compression struts with very large axial stiffness but low deformability. As a result, the lateral force demand of the straight-run

Table 4
Performance parameters of the *Baseline Model*.

Loading direction		K_e (kN/mm)	Δ_y (mm) [%]	F_y (kN)	F_u (kN)	Ω	$\Delta_{long}^{landing}$ (mm) [%]	$\Delta_{trans}^{landing}$ (mm) [%]
Parallel	(+)	1.1	10.7 [0.3]	10.5	55.1	5.2	60 [1.6]	71 [1.9]
	(−)	1.2	11.1 [0.3]	12.0	55.3	4.6	106 [2.9]	65 [1.8]
Transverse	(+)	0.7	13.2 [0.4]	7.1	21.0	2.9	20 [0.6]	6 [0.2]
	(−)	0.6	17.2 [0.5]	8.4	24.0	2.8	19 [0.5]	39 [1.0]

Values in square brackets represent the percentile displacement with respect to story height.

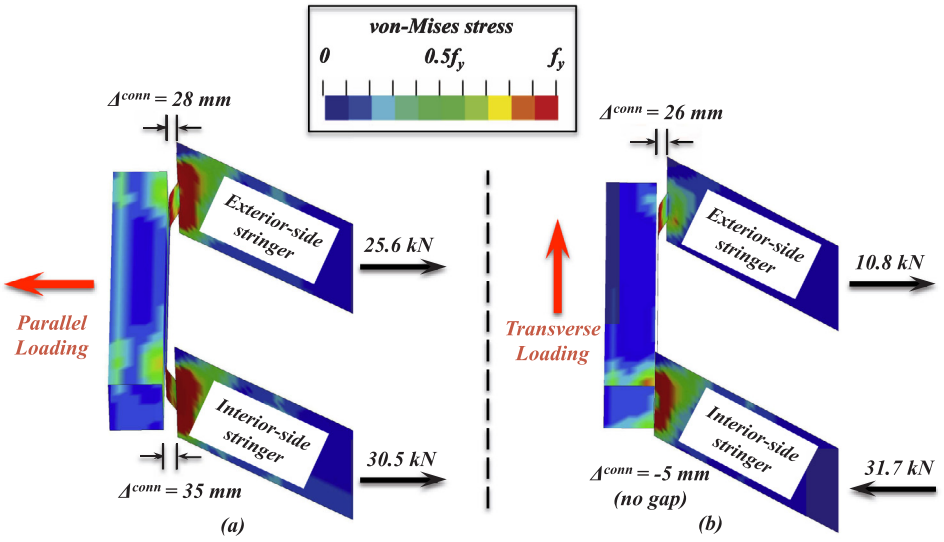

Fig. 10. Upper floor connection deformation and stringer axial forces of the *Baseline Model* at the ultimate state (2.5% IDR): (a) parallel loading, and (b) transverse loading.

stair is more than an order of magnitude larger than that of the *Baseline Model*. For this reason, the performance parameters of the straight-run stair under the compressive parallel loading are not presented in Fig. 11g.

4.3. Connection response

Since the stair connections sustain larger force and displacement demands in the case of parallel loading, it represents a more critical loading scenario for evaluating the seismic behavior of the stairs. In this regard, result discussions focus on the connection behavior under loading in this direction. Although weld fracture is not explicitly considered in the models, the predicted stresses and strains are used to assess the weld behavior of the stairs with different connection details. Specifically, the principal stress is used as an indicator for brittle fracture potential, since this type of failure usually occurs abruptly and is not always accompanied with significant plastic deformations [21]. Additionally, the plastic equivalent strain is used as a measure of the local strain demands on the connection welds [22].

Fig. 12 presents the force-deformation response of the upper floor connections for parallel loading as well as the connection deformed shapes at the ultimate state (2.5% IDR). Since the lower floor connections are all rigid connections, their responses are not presented in the figure but rather summarized in Table 5. Fig. 12 indicates that the deformable connections (*Baseline Model* and Case 6) both elongate by more than 30 mm at the ultimate state (accounting for more than one third of the interstory drift), whereas the deformation of the rigid connection (Case 7) remains small (< 5 mm). Initial yielding of the deformable connections occurs when the deformation remains small (5–10 mm). However, the rigid connection does not experience salient yielding at the connection per se, since plastic deformation localizes at the tip of the vertical weld on the interior stringer side (and instead first yield occurs on the flight-to-landing connections). It is also observed that the rigid connection force is about 30% higher than those of the deformable connections at the ultimate state.

Unlike structural members whose post-yield behavior is often characterized by well-studied overstrength and ductility factors, the (deformable) connection force increases monotonically following initial yielding due to stiffness hardening of the connection under large deformation (Fig. 12). The connection forces at the ultimate state attain five times as much as those at the initial yield state (also see Table 4) and may continue to increase until the occurrence of eventual physical damage (e.g., connection weld fracture as reported in [11]). In this regard, future experimental studies would benefit from investigating the ultimate deformability of the connections, while restraining their force in a more controlled manner.

Table 5 summarizes the upper and lower connection deformations as well as the stress and strain response of the vertical fillet welds at the ultimate state (2.5% IDR) in the parallel direction. It is noted that the stairs with deformable upper connections (*Baseline Model* and Case 6) experience similar weld stress and strain response. Compared with the corresponding lower connection welds, the upper connection welds attain slightly larger maximum principal stresses (about 10%) but much smaller effective plastic strains (as low as 30%). The plastic strains of the deformable upper connections tend to distribute more evenly via plastic yielding at both ends of the deformable connections (Fig. 12). In contrast, the rigid upper connection welds (Case 7) sustain the largest effective plastic strain among all three models (about 5 times as much as those of the deformable upper connections). Due to its limited deformability, the plastic strain tends to localize at the tip of the vertical weld on the interior stringer side, while the weld at the other side remains elastic (Fig. 12). As a result of the largest connection force among all three models, the maximum principle stress of the rigid upper connection welds is also the highest. The apparently larger stress and strain demands indicate that the rigid upper connection (Case 7) is subjected to the highest potential of connection weld fracture.

5. Conclusions

Despite the significance of stair systems related to occupant evacuation and post-event recovery operations following an earthquake, past events repeatedly demonstrate the seismic vulnerability of these critical nonstructural systems. Their seismic behavior is complex due to their variability in spatial geometry and construction details. This paper presents a computational study of the seismic response of prefabricated steel stair systems with a focus on scissors configured stairs. To this end, a high fidelity three-dimensional finite element model is first developed and validated against prior experimental results. A parametric study is subsequently performed to explore the impact of loading directions as well as critical design variables on the lateral force-displacement response of the stairs and the connection behavior. Design variables considered in this study include story height, landing post configuration, connection details, and geometric configuration. Based on the parametric analysis of eight stair models, key findings are summarized

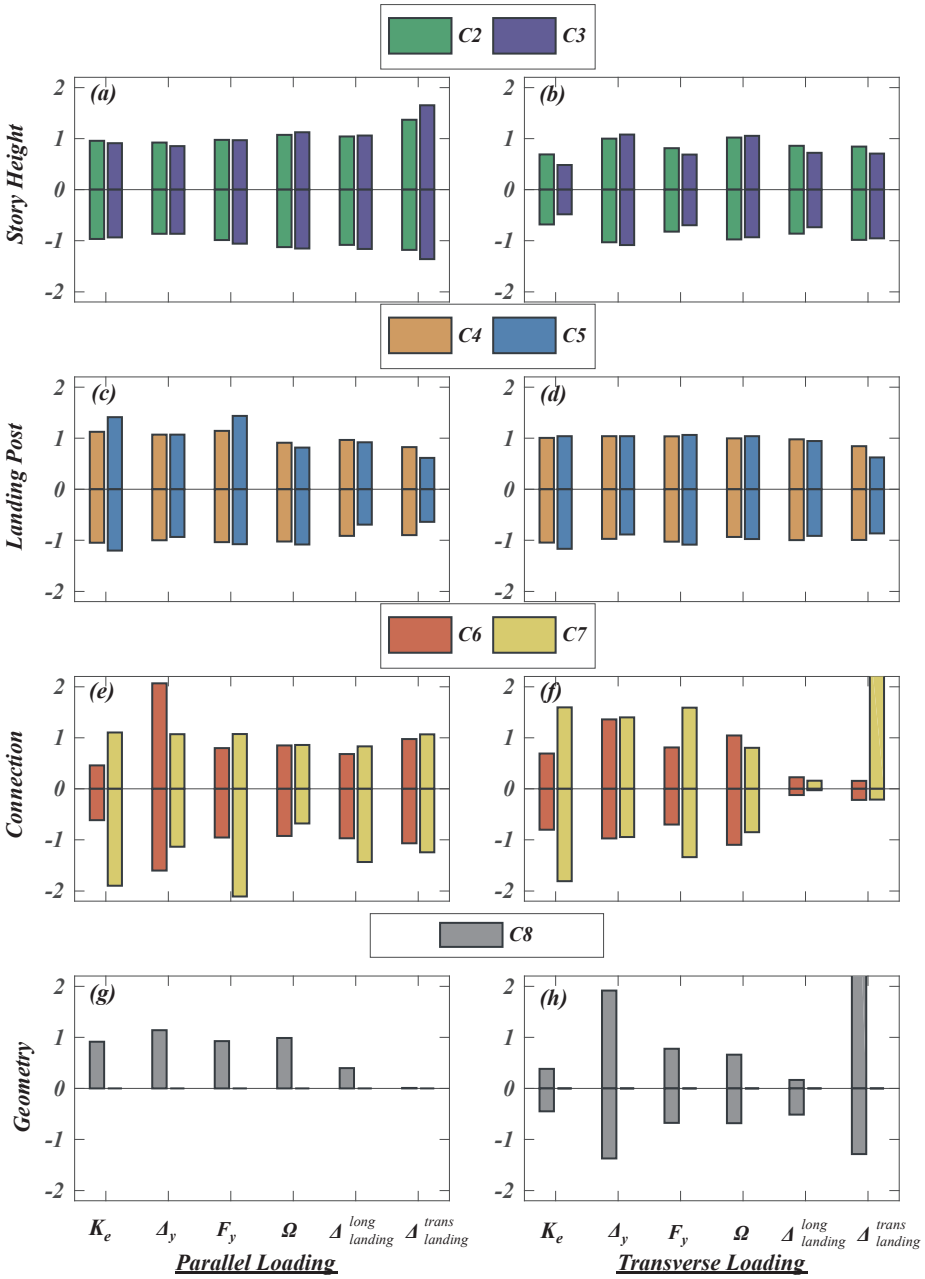

Fig. 11. Normalized stair performance parameters under parallel and transverse loading (design variables are denoted on the y-axis).

as follows:

1. The seismic behavior of the stair differs significantly between loading in the two horizontal directions. The stair attains larger forces and relative landing displacements when loading is applied in the parallel direction. The upper flight resembles an inclined axial member in the case of parallel loading, thus imposing large displacement demands on the landing and connections. In the case of transverse loading, the upper flight tends to perform as a flexural member, which effectively enhances the overall deformability and reduces the force demands of the stair. The selection of loading of course will be irrespective and may occur in sync, due to the natural bi-directional nature of an earthquake; nonetheless, these studies allow an understanding of the most critical conditions and potential design pitfalls that should be considered in practice.
2. Among the four design variables considered in the parametric study, the seismic behavior of the stairs appear most sensitive to the variation in connection details and geometric configurations. Variation of these parameters substantially modifies the overall deformation mechanisms of the stair as a system.
3. As a result of stiffness hardening of the deformable connections under large deformation, the connection force may continue to increase until the occurrence of eventual physical damage. Future experimental studies are needed to investigate the ultimate connection deformability and restrain their force limits in a more controlled manner. Capacity design principles, as commonly adopted for designing structural components, would allow more optimal control of the stair behavior in this regard.
4. Due to large stress and strain demands, the stair with rigid connections at both the upper and lower floors is subjected to the highest potential of weld fracture. Clearly, future designs should avoid the simultaneous use of rigid stair connections at the top and bottom floors.

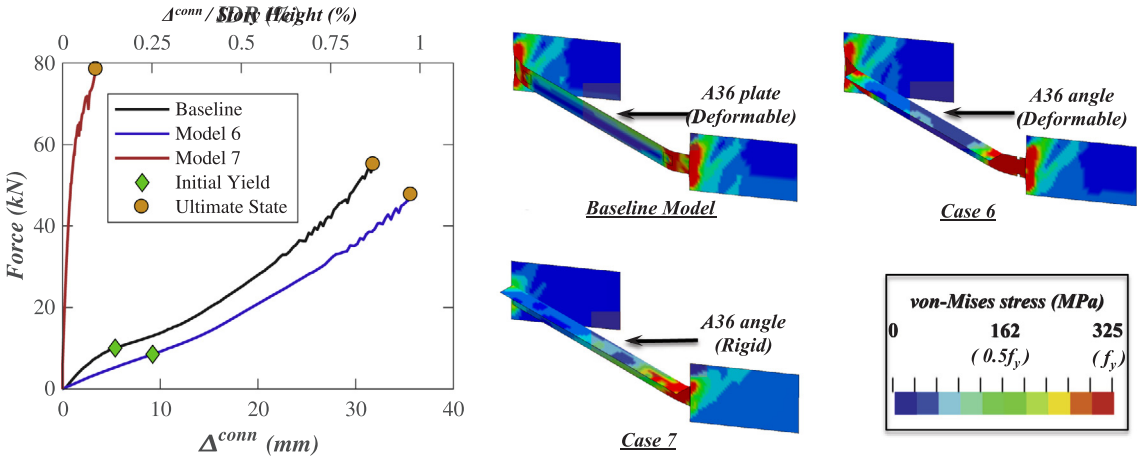

Fig. 12. Upper floor connection force-deformation response for parallel loading and the deformed shapes of the connections at the ultimate state (2.5% IDR).

Table 5
Flight-to-building connection weld stress and strain response and connection deformation at the ultimate displacement loading in the parallel direction.

Model	Connection location	σ_1 (MPa)	ε_p	$\Delta^{connection}$ (mm)
Baseline (Case 1)	Upper	396	0.031	31.8
	Lower	352	0.089	4.2
Case 6	Upper	388	0.033	35.9
	Lower	354	0.074	3.6
Case 7	Upper	470	0.155	4.5
	Lower	362	0.093	4.0

σ_1 = maximum principle stress; ε_p = plastic equivalent strain; $\Delta^{connection}$ = average connection deformation (elongation) in the parallel direction.

The computational parametric study provides insight into the complex seismic behavior of prefabricated steel stairs under pseudo-static uniaxial displacement loading. It reaffirms the importance of connections While also highlighting the impact of select design aspects on the seismic behavior of stair systems. It is noted, however, that this study primarily focuses on lightweight steel stairs in a scissors arrangement. Such systems have demonstrated poor performance in recent earthquakes with their behavior dominated by differential displacements and sensitive to landing torsion. Further investigation is needed to better understand the response characteristics of stairs configured in other geometric layouts (e.g., straight-run) or constructed with more brittle materials (e.g., reinforced concrete) as well as the effects of dynamic loading on stairs, in particular heavier stairs or stairs with their frequencies closely tuned with those of the supporting structures.

Acknowledgements

This study was supported by the National Science Foundation through Grant No. CMMI-0936505, “Full-Scale Structural and Nonstructural Building System Performance during Earthquakes”. The first author also received partial support through a dissertation fellowship from the Department of Structural Engineering at the University of California, San Diego. The authors also appreciate the input of Professor Joel Conte during the developments of the model. The above support is gratefully acknowledged. Opinions and findings of this study are of the authors and do not necessarily reflect those of the sponsors.

References

[1] FEMA-E74. Reducing the risks of nonstructural earthquake damage – a practical guide. Washington, DC: Federal Emergency Management Agency; 2014.
[2] ICC. International building code. Washington, DC: International Code Council; 2012.
[3] NIST. Recommendations for seismic design of reinforced concrete wall buildings based on studies of the 2010 Maule, Chile Earthquake. NIST GCR 14-917-25. Gaithersburg (MD): National Institute of Standards and Technology; 2014.
[4] ASCE 7-10. Minimum design loads for buildings and other structures. Reston (VA): ASCE/SEI 7-2010; 2010.
[5] Roha C, Axley JW, Bertero VV. The performance of stairways in earthquakes. UCB/EERC-82/15. Berkeley (CA): Earthquake Engineering Research Center, University of California Berkeley; 1982.
[6] Bull DK. Stair and access ramps between floors in multi-storey buildings. A report of the Canterbury Earthquakes Royal Commission, Christchurch, New Zealand; 2011.
[7] Li B, Mosalam KM. Seismic performance of reinforced-concrete stairways during the 2008 Wenchuan earthquake. ASCE J Perform Constr Facil 2013;27(6):721–30.
[8] Rojas F, Naeim F, Lew M, Carpenter LD, Youssef NF, Saragoni GR, et al. Performance of tall buildings in Concepción during the 27 February 2010 moment magnitude 8.8 offshore Maule, Chile earthquake. Struct Des Tall Special Build 2011;20(1):37–64.
[9] Simmons PW, Bull DK. The safety of single storey straight stairflights with mid-height landings under simulated seismic displacements. Research report 2000–09. Christchurch (New Zealand): Department of Civil Engineering, University of Canterbury; 2000.
[10] Higgins C. Prefabricated steel stair performance under combined seismic and gravity loads. ASCE J Struct Eng 2009;135(2):122–9.
[11] Wang X, Astroza R, Hutchinson T, Conte J, Restrepo J. Dynamic characteristics and seismic behavior of prefabricated steel stairs in a full-scale five-story building shake table test program. Earthquake Eng Struct Dyn 2015;44(14):2507–27.
[12] Chen MC, Pantoli E, Wang X, et al. Full-scale structural and nonstructural building system performance during earthquakes: Part I – Specimen description, test protocol and structural response. Earthquake Spectra 2016;32(2):737–70.
[13] Cosenza E, Verderame GM, Zambrano A. Seismic performance of stairs in the existing reinforced concrete building. In: Proc 14th world conference on earthquake engineering, Beijing, China; 2008.
[14] Tegos IA, Panoskaltsis VP, Tegou SD. Analysis and design of staircases against seismic loadings. In: 4th ECCOMAS thematic conference on computational methods in structural dynamics and earthquake engineering, Kos Island, Greece; 2013.
[15] LSTC. LS-DYNA keyword user’s manual – volume 1 (Version 971). Livermore (CA): Livermore Software Technology Corporation; 2013.
[16] LSTC. LS-DYNA keyword user’s manual – Volume 2 (Version 971). Livermore (CA): Livermore Software Technology Corporation; 2013.
[17] ANSI/AISC 341-16. Seismic provisions for structural steel buildings. Chicago (IL): American Institute of Steel Construction; 2016.
[18] Liu J. Updates to expected yield stress and tensile strength ratios for determination of expected member capacity in the 2016 AISC seismic provisions. AISC Eng J 2016;53(4):215–28.
[19] Yoshida F, Uemori T. A model of large-strain cyclic plasticity describing the Bauschinger effect and workhardening stagnation. Int J Plast 2002;18(5):661–86.
[20] Jia LJ, Kuwamura H. Prediction of cyclic behaviors of mild steel at large plastic strain using coupon test results. ASCE J Struct Eng 2014;140(2):04013056.
[21] Kanvinde AM, Deierlein GG. Cyclic void growth model to assess flexible fracture initiation in structural steels due to ultra low cycle fatigue. ASCE J Eng Mech 2007;133(6):701–12.
[22] Kanvinde AM, Fell BV, Gomez IR, Roberts M. Predicting fracture in structural fillet welds using traditional and micromechanical fracture models. Eng Struct 2008;30(11):3325–35.
[23] El-Tawil S, Mikesell T, Kunnath SK. Effect of local details and yield ratio on behavior of FR steel connections. ASCE J Struct Eng 2000;126(1):79–87.
[24] Mao C, Ricles J, Lu LW, Fisher J. Effect of local details on ductility of welded moment connections. ASCE J Struct Eng 2001;127(9):1036–44.
[25] Wang X. Experimental and computational investigation of the seismic behavior of stair systems in buildings. Ph.D. dissertation. La Jolla (CA): University of California San Diego; 2015.